American Journal of Engineering Research (AJER)
e-ISSN: 2320-0847 p-ISSN : 2320-0936
Volume-13, Issue-3, pp-55-64
www.ajer.org
Research Paper Open Access

Accuracy and angular limit of the aerodynamic profile at the central inlet of standard wind turbine sensors

Ulrich Canissius[1]*, Nirinarison Jean Razafinjaka[2]
[1] *Laboratoire de Mécanique et de Métrologie - LMM, Ecole Normale Supérieure pour l'Enseignement Technique - ENSET*
Antsiranana University, B.P.O, Madagascar
**Corresponding Author: ulrich_canissius@yahoo.fr*
[2] *Ecole Doctorale Thématique, Energies Renouvelables et Environnement - EDT-ENRE*
Antsiranana University, B.P.O, Madagascar

ABSTRACT: *In this paper, the authors bring an element of performance to the angular limit of the central shield of the aero-motor. Through an implicit finite-difference scheme, they numerically solve the permanent, laminar and three-dimensional transfer equations between an isothermal body of revolution and a Newtonian fluid considered in upward flow generated by natural, forced, rotational and coupled two-by-two convections. The lack of scientific literature on this subject prompted the authors to make a contribution. The aim is to provide an element of performance to the airflow channeling device that conveniently appears in conical or elliptical form at the central inlet of the usual sensors on modern wind turbines.*
KEYWORDS: *aero-motor, external convection, aerodynamic behavior, ellipse and cone of revolution, angular limit.*

Date of Submission: 10-03-2024 Date of acceptance: 23-03-2024

NOMENCLATURE

Roman letter symbols

a thermal diffusivity of the fluid, [$m^2.s^{-1}$]
a' length of the semi-axis, according to the length: case of ellipsoid, [m]
b length of the semi-axis, perpendicular to the axis of revolution, [m]
b' length of the half-axis of the truncated base of the ellipsoid, perpendicular to the axis of revolution, [m]
Cf_u meridian friction coefficient
Cf_w azimuthal friction coefficient
Cp specifique heat capacity at constant pressure of the fluid, [$J.kg^{-1}.K^{-1}$]
Gr dimensionless Grashof number
L length of the reference body (cone, ellipsoid), [m]
Nu local Nusselt number
Pr Prandtl number
r normal distance between the M projection from a point P to the axis of revolution, [m]
S_x,S_φ geometric configuration factors
T_∞ fluid temperature away from the wall, [K]
T_p wall temperature, [K]
V_x velocity component in x direction, [$m.s^{-1}$]
V_y velocity component in y direction, [$m.s^{-1}$]
V_φ velocity component in φ direction, [$m.s^{-1}$]
x, y meridian and normal coordinates, [m]

Greek letter symbols

α body inclination angle, [°]
α_e eccentric angle in the literature: case of an ellipsoid, [rad]

φ azimuthal coordinate, [°]
ν kinematic viscosity, [$m^2.s^{-1}$]
λ thermal conductivity, [$W.m^{-1}.K^{-1}$]
β volumetric coefficient and thermal expansion, [K^{-1}]
μ dynamic viscosity [$kg.m^{-1}.s^{-1}$]
θ_o half angle of the cone: case of a cone, [°]

Indice/Exponent
$+$ dimensionless variables

I. INTRODUCTION

In this treatise, we offer a clarification of the angular limit that was previously proposed [1], with the aim of better concretizing its range of use and offering new knowledge to the community of researchers and players in the field.
Many researchers are investing in the physical and aerodynamic behavior of the wind sensor, but until now, one rarely finds work focusing on the necessity and performance of the commonly used conical or elliptical shape of the nose of these wind turbines (figure 1).
Among the numerous authors listed in this field, the works deal more with the conceptual aspect of sensors, and the scientific concept of these remains solely in the observation leading to correlation or law at the whim of each, usually, to meet the subjective and hypothetical perception of their project.

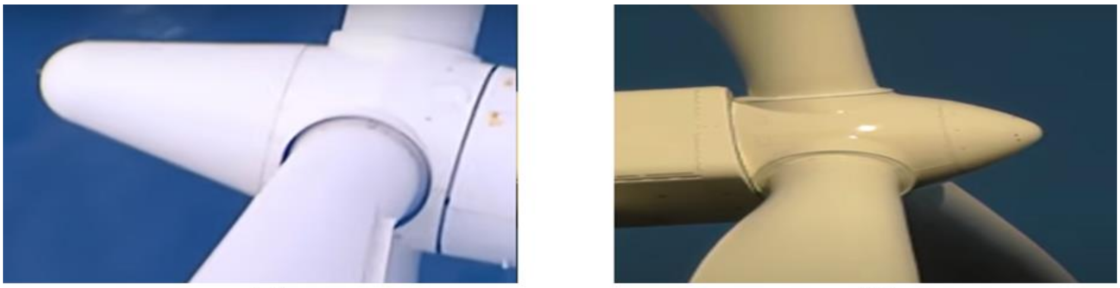

(a) (b)

Figure 1. Illustrative profile images, [2]
(a): elliptical shaped device; (b): conical shaped device

However, the profile in question conveniently represents the wind turbine nose, attenuating the disturbance caused by the central depression. It contributes to the turbine's stability by channeling the central air flow to the sensors. This disturbance can influence not only the design of the mast or a sub-assembly of the infrastructure, but also the economic dimension of the structure.

Furthermore, given the complexity of the flow around the collectors, a mathematical model is proposed for its resolution. In such a situation, the Navier-Stokes equations will be used for this purpose, with simplifying assumptions facilitating resolution of the system of equations, continuity, momentum and heat.

II. THEORETICAL FRAMEWORK

The scientific concept of the subject is based on the thermodynamic relationship between an isothermal body of revolution and a fluid flowing through it. The general relationship between the solutions of an axisymmetric system of an isothermal body has been developed by Merk and Prins [3] since 1953. The authors studied natural laminar thermal convection of the boundary layer type in the vicinity of a cone with a smooth surface. They observed that the surface condition of the body contributes to the transfer performance, with roughness attenuating the exchange. Authors such as Alamgir [4] and Bapuji [5] investigated on the global heat transfer in unsteady laminar natural convection from an isothermal vertical cone using the integral method.

Hossain and his contributor [6] analyzed the effects of transpiration velocity on laminar boundary layer flow by free convection around a vertical non-isothermal cone and showed that due to increasing temperature gradient, both velocity and surface temperature decrease. Up to now, many authors have dealt with thermodynamic problems around bodies of revolution (spheres, cones and ellipses) immersed in two- or three-dimensional, linear or rotational flow [7 - 15], but without any alliances with practical reality. What's more, work on the typological coupling of convections influencing the variability of fluid physical properties [16 - 20], contributes very little to the techno-scientific desire, to societal and social demand, precisely, the practical side of research.

Considering all these services, our ambition is to contribute to the aerodynamic performance of the usual wind turbine sensors, through a new scientific understanding that demystifies the need for conditioned use of the profile in question, located at the central inlet of the aero-motor.

III. THEORETICAL FOUNDATIONS

The physical model consists of a body of revolution (cone and ellipsoid) of length L, inclined at an angle α or not to the vertical. The wall of the body is maintained at a constant temperature Tp, different from the temperature T∞ of the fluid away from the wall, which is also constant. Figure 2 shows the spatial configuration of the physical model of the system under study.

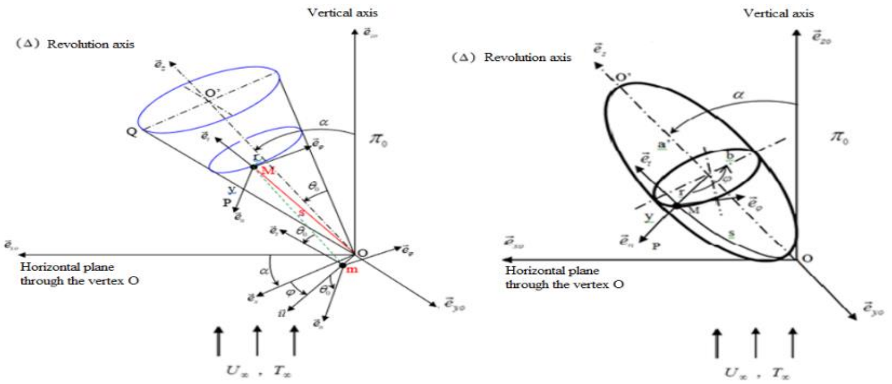

Figure 2. Physical model and co-ordinates system

Generally, in turbines, each time the wind direction changes, the profile changes position from one instant to the next, under the effect of the directional control device or rudder and, at the repeated instant t, the flow remains inclined by a varied angle α before this profile is reoriented, and the reason for this configuration.

IV. CONSERVATION EQUATIONS

The equations are the same for both body types. We present only the case of natural convection, in order to soften the reading, and supplement it with references and our published work (forced, rotatory and three two-by-two couplings of the three convections).

Case of pure natural convection

We pose $\Delta T = T_p - T_\infty$, and the appropriate reduced variables are [21, 31]:

$$x_+ = \frac{x}{L},\ y_+ = \frac{y}{L}Gr^{\frac{1}{4}},\ \varphi_+ = \varphi,\ V_x^+ = \frac{V_x}{\sqrt{Lg\beta\Delta T}},\ V_y^+ = \frac{V_y Gr^{\frac{1}{4}}}{\sqrt{Lg\beta\Delta T}},\ V_\varphi^+ = \frac{V_\varphi}{\sqrt{Lg\beta\Delta T}},\ r^+ = \frac{r}{L} \text{ and } T^+ = \frac{T-T_\infty}{T_P-T_\infty} \tag{1}$$

Continuity, momentum and heat equations

$$\frac{\partial V_x^+}{\partial x_+} + \frac{\partial V_y^+}{\partial y_+} + \frac{1}{r^+}\frac{\partial V_\varphi^+}{\partial \varphi_+} + \frac{V_x^+}{r^+}\frac{dr^+}{dx_+} = 0 \tag{2}$$

$$V_x^+\frac{\partial V_x^+}{\partial x_+} + V_y^+\frac{\partial V_y^+}{\partial y_+} + \frac{V_\varphi^+}{r^+}\frac{\partial V_x^+}{\partial \varphi_+} - \frac{V_\varphi^{+2}}{r_+}\frac{dr^+}{dx_+} = S_x T^+ + \frac{\partial^2 V_x^+}{\partial y_+^2} \tag{3}$$

$$V_x^+\frac{\partial V_\varphi^+}{\partial x_+} + V_y^+\frac{\partial V_\varphi^+}{\partial y_+} + \frac{V_\varphi^+}{r^+}\frac{\partial V_\varphi^+}{\partial \varphi_+} + \frac{V_x^+ V_\varphi^+}{r^+}\frac{dr^+}{dx_+} = S_\varphi T^+ + \frac{\partial^2 V_\varphi^+}{\partial y_+^2} \tag{4}$$

$$V_x^+\frac{\partial T^+}{\partial x_+} + V_y^+\frac{\partial T^+}{\partial y_+} + \frac{V_\varphi^+}{r^+}\frac{\partial T^+}{\partial \varphi_+} = \frac{1}{Pr}\frac{\partial^2 T^+}{\partial y_+^2} \tag{5}$$

With $Pr = \frac{\mu Cp}{\lambda} = \frac{\nu}{a}$ and $Gr = \frac{g\beta(T_p - T_\infty)L^3}{\nu^2}$

Nusselt number and friction coefficients expressions

$$NuGr^{-\frac{1}{4}} = -\left(\frac{\partial T^+}{\partial y_+}\right)_{y_+=0};\ Cf_u = Lc_f\left(\frac{\partial V_x^+}{\partial y_+}\right)_{y_+=0} \text{ and } Cf_\varphi = Lc_f\left(\frac{\partial V_\varphi^+}{\partial y_+}\right)_{y_+=0} \tag{6}$$

Lc_f represents a coefficient which results from the adimensionalization.

Conditions to the limits

At the wall, $y_+ = 0,\ T^+ = 1, V_x^+ = 0, V_y^+ = 0$ and $V_\varphi^+ = 0$ (7)

Away from the wall, $y_+ \to \infty, T^+ \to 0, V_x^+ \to 0, V_y^+ \to 0$ and $V_\varphi^+ \to 0$ (8)

The conservation equations, the reference quantities suitable for adimensionalization and boundary conditions dealing with pure forced convection, pure rotatory convection and couplings thereof are given in our work [22, 23, 24, 25, 26, 27].

V. METHODOLOGY AND MODELING

The dimensionless transfer equations are discretized using the finite-difference method in its implicit form. The body wall is divided into small curvilinear elementary surfaces using Np and Mn, which represent the parallels perpendicular to the axis of revolution OO' and the meridians passing through the poles O and O'. The points of intersection of these parallels and meridians define the nodes of the mesh, from which calculations are made from the wall towards the bosom of the fluid along the normal. The study domain is decomposed into N x M x L curvilinear parallelepipeds attached to the body and defined by the dimensionless pitches Δx_+, Δy_+ and $\Delta\varphi_+$. In this case, L and N are fixed in advance, as they are directly linked to the geometric discretization of the body. However, for a given stack and indexed by p, the thickness of the boundary layer is not known in advance and the index (JMAX)p characterizes the thickness and changes a priori from one stack to another. Then, M is defined by the relation:

$$M = \sum_{p=1}^{L \times N} (JMAX)p \tag{9}$$

Calculations are performed at nodes (i+1, j, k), with $1 \le i \le IMAX$, $1 \le j \le JMAX$ and $1 \le k \le KMAX$. For the dimensionless quantities $V_x^+, V_y^+, V_\varphi^+$ and T^+, we approximate the partial derivatives as follows, with X denoting one of them and the unknowns being the quantities denoted by i+1.

The terms V_x^+, V_y^+ and V_φ^+ in the operators $V_x^+ \frac{\partial}{\partial x_+}$, $V_y^+ \frac{\partial}{\partial y_+}$ and $V_\varphi^+ \frac{\partial}{\partial \varphi_+}$ are respectively replaced by the values $(V_x^+)_{i+1,j}^k$, $\left(V_y^+\right)_{i+1,j}^k$, $\left(V_\varphi^+\right)_{i+1,j}^k$ and calculated at nodes (i+1, j, k).

We denote by U, V, W and T the meridional, normal and azimuthal components and the dimensionless temperature. The discretized equations can be written as follows:

$$AX_{j+1} + BX_j + CX_{j-1} = D_j,\ \text{for } 2 \le j \le J\max - 1 \tag{10}$$

The algebraic systems (10) associated with the discretized boundary conditions are solved using the Thomas algorithm. The dimensionless normal component V_y^+, is obtained from the discretization of the continuity equation:

$$\begin{cases} V_{i+1,j}^k = \frac{1}{4}[A' + B'] \\ A' = 3V_{i+1,j+1}^k + V_{i+1,j-1}^k \\ B' = 2\Delta y_+ \left(\frac{U_{i+1,j}^k - U_{i,j}^k}{\Delta x_+} + \frac{3W_{i+1,j}^{k+1} - 4W_{i+1,j}^k + W_{i+1,j}^{k-1}}{2\Delta\varphi_+ r_{i+1}^+} + \frac{U_{i+1,j}^k}{\Delta x_+}\left(1 - \frac{r_i^+}{r_{i+1}^+}\right)\right) \end{cases} \tag{11}$$

With $1 \le i \le N-1$, $1 \le k \le L-1$ and $2 \le j \le J\max - 1$

We have taken a precision $\varepsilon = 10^{-6}$, and the convergence criterion within the boundary layer is assured when:

$$\left| \frac{|(X)^{p+1}| - |(X)^p|}{\mathrm{Sup}(|(X)^{p+1}|, |(X)^p|)} \right| \le \varepsilon \tag{12}$$

$(X)^p$ and $(X)^{p+1}$ are the values of the quantity X at iteration p and p+1 respectively.

VI. RESULTS AND DISCUSSION

The phenomenon of a neutral point is often visible on the dimensionless normal speed on which all parameters have no effect at a defined point on the surface. This point represents another avenue of investigation into the performance of an aerodynamic profile for the community of actors, but in this paper, we will present in part the physical meaning of it.

The inclination of the body and the opening at the top, in the case of a cone, contribute strongly to the variability of the intensities of all the dimensionless quantities. However, the evolution of these magnitudes around an ellipsoid is limited in the case of free convection, enabling us to witness and corroborate the events observed through a cone. The recommendation or need to use the questioned profile on the usual wind turbine sensors, particularly those with horizontal axes, would be substantiated. The calculation code is validated with Lin (1976) for the case of a cone (figure 3) and with Jaman (2010) for the case of an ellipsoid (table 1).

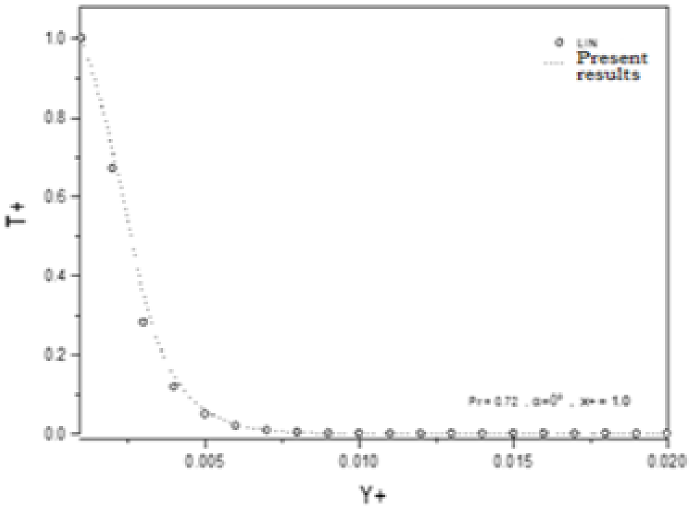

Figure 1. Our results and those deduced from the literature (Lin).
Steady-state temperature against y+, Pr=0.72, x+=1.0 and α=0°.
Case of the cone

Tableau 1. Our results and those deduced from the literature (Jaman).
Exchange coefficient, $\alpha_e \in [0, \pi]$, Pr=1.0 and b/a=0.25.
Ellipsoid case

α_e	Present results	M.K. Jaman *et al.* (2010)
0.0	0.8412	0.8426
0.2	0.7714	0.7706
0.4	0.6622	0.6619
0.6	0.5790	0.5781
0.8	0.5184	0.5175
1.0	0.4736	0.4729
1.2	0.4397	0.4392
1.4	0.4146	0.4132
1.6	0.3936	0.3929
1.8	0.3772	0.3768
2.0	0.3644	0.3641
2.2	0.3539	0.3538
2.4	0.3450	0.3451
2.6	0.3368	0.3370
2.8	0.3264	0.3270
3.0	0.3072	0.3062
π	0.2782	0.2780

The ranges limiting the opening at the top of the cone are obtained from a repeated, criterion-referenced simulation of two dynamic quantities, [31]:

$\theta_{0\ limit} = \pi/2 - (\alpha-1)$ and $\theta_{0\ limit} \geq \alpha+1$ (normal and tangential) (13)

The dimensionless normal component appears negative for $\theta_0 < \alpha$ on the lower meridian of equation $\varphi = 0°$ and contrary on the upper meridian. This indicates the presence of suction in the azimuthal position defined by $\varphi = 0°$ (Figure 5.a), and of a slight detachment of particles at $\varphi = 180°$ (Figure 5.b). On the other hand, in the interests of good stability and knowing that $\alpha = f(\theta_0)$, we adopted the conditions defined by relationship (13). Following the linear projection of the stopping point towards the base of the truncated part of the ellipsoid (a'>b'), 2b' is proportional to 2r of the large base of the cone, as shown in figure 4.

The author and his contributor used an elongated ellipsoid since b represents the vertical half-axis of revolution in their configuration. In ours, a' represents the latter, and b' is the length of the half-axis of the truncated base of the ellipsoid, perpendicular to the horizontal axis of revolution and parallel to b.
Furthermore, in results based on the elliptical profile, let's note a'=a and b=c to soften the reading.

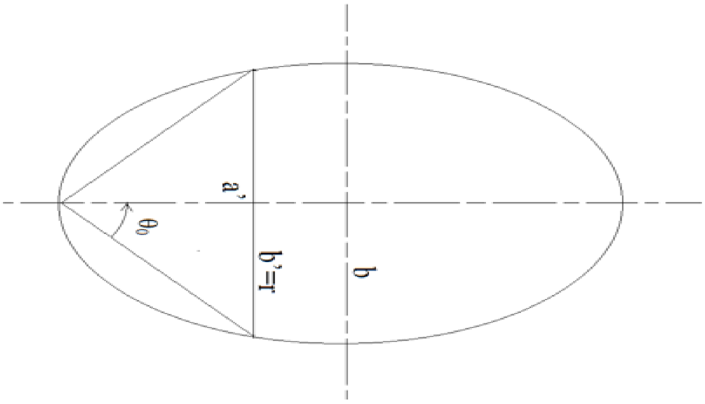

Figure 4. Configuration of profile shape and position parameters

In this article, we focus on the dimensionless normal component, due to the high frequency of its appearance as a function of the variability of physical parameters. The dimensionless velocity V+ is generally the most significant dynamic quantity in fluid mechanics.

Figure 5.a shows variations in the dimensionless normal component on the first parallel. The curves suggest an expansive negative pole as the profile opening angle increases. The presence of suction of the fluid towards the wall causes a slight depression to develop on the trunk of the body. In this figure, the disappearance of this phenomenon starts from the equilibrium between the two angles, i.e. $\theta_0 = \alpha$. As a precaution, in order to ensure good stability taking into account the related hypothesis, we will limit the ranges of use of the opening angle by the aforementioned relationship. However, on the upper meridian defined by $\varphi = 180°$, this component always appears positive over wide ranges of aperture from 0° to 90°, and tilt from 10° to 45° (figure 5.b).

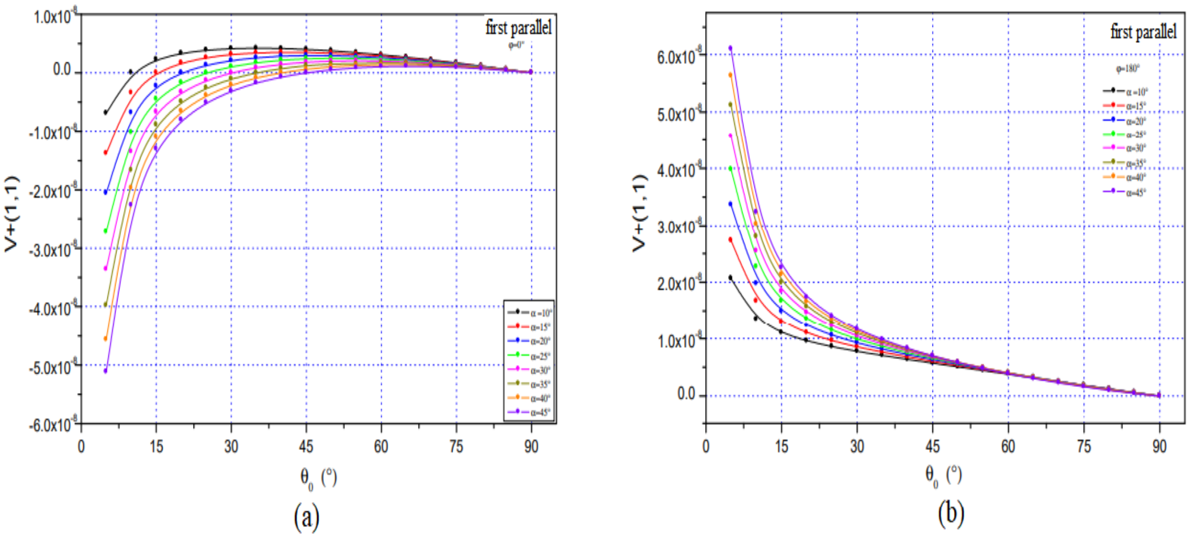

Figure 5. Variations in the dimensionless normal component U+, against the opening angle at the top of the cone, for several values of α at the lower and upper meridians
(a): for α=10° to 45°, with θ_0=0° to 90° and φ=0°
(b): for α=10° to 45°, with θ_0=0° to 90° and φ=180°

The modulus of the normal velocity is important depending on the increase in the angle of inclination, and the magnitude of this causes a strong suction certainly causing a depression and also generates a disturbance of fluid at the inlet central (figure 6). As for the growth of the a/c ratio, it amplifies the suction of the fluid towards the wall following the dimensionless normal direction (figure 7.b). In addition, this growth contributes to the amplitude of the pulsation following the dimensionless meridian direction (figure 7.a).

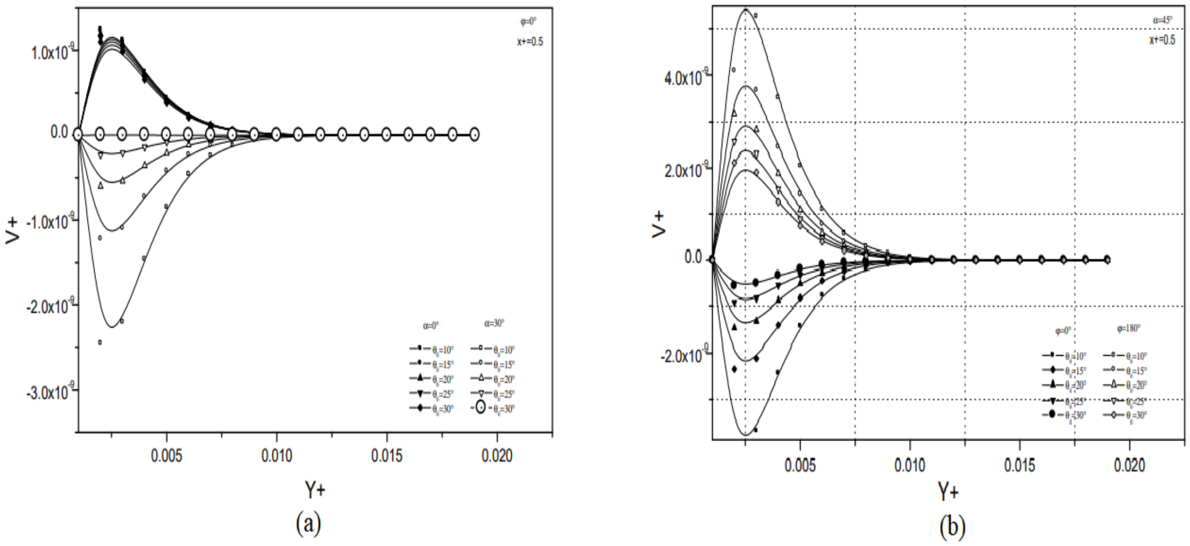

Figure 6. Variations of the dimensionless normal component V+ against the dimensionless normal coordinate y+, for several values of θ_0, α and x+=0.5
(a) : for φ=0°, α=0° and 30°, θ_0=10° - 30°
(b) : for φ=0° and 90°, α=45°, θ_0=10° - 30°

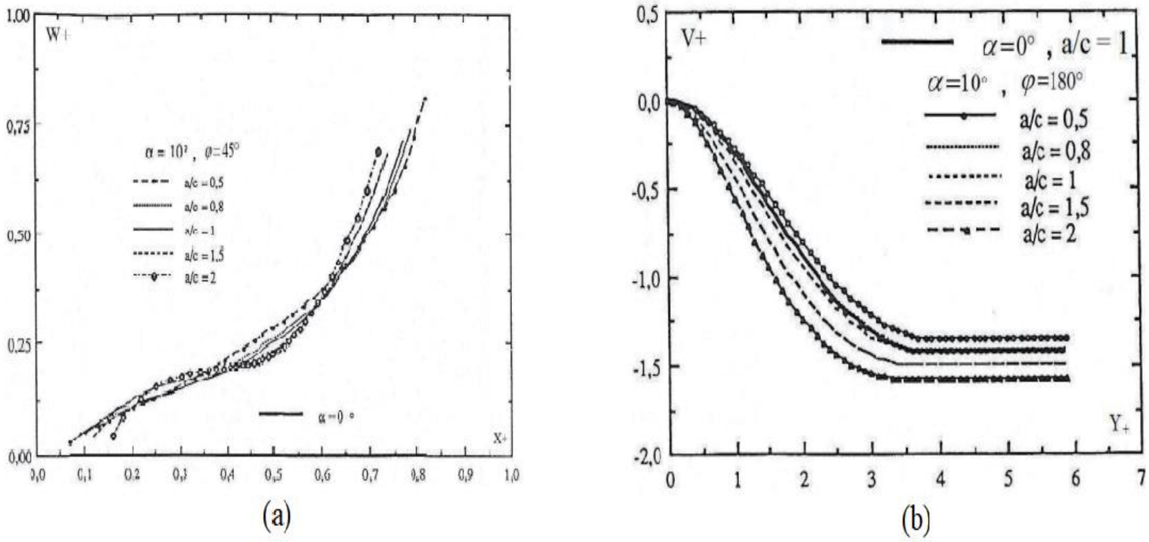

Figure 7. Variations of the dimensionless normal component V+ as a function of the dimensionless meridian and normal coordinates, for several values of a/c
(a) : V+ against x+, φ=45°, α=10° and a/c= 0.5, 0.8, 1, 1.5, 2
(b) : V+ against y+, φ=180°, α=10° and a/c= 0.5, 0.8, 1, 1.5, 2

Concerning the dimensionless temperature in the pure natural case, the physical parameters have very little influence on it, and Figure 8.a corroborates this observation. In figure 8.b, the inverse consequence of the adhesion intensity seems to be seen, and the increase in the opening and the inclination of the body attenuates this magnitude, i.e., the decrease in the negative value indicates that the tangential friction is reduced as a function of the growth of α and θ_0.

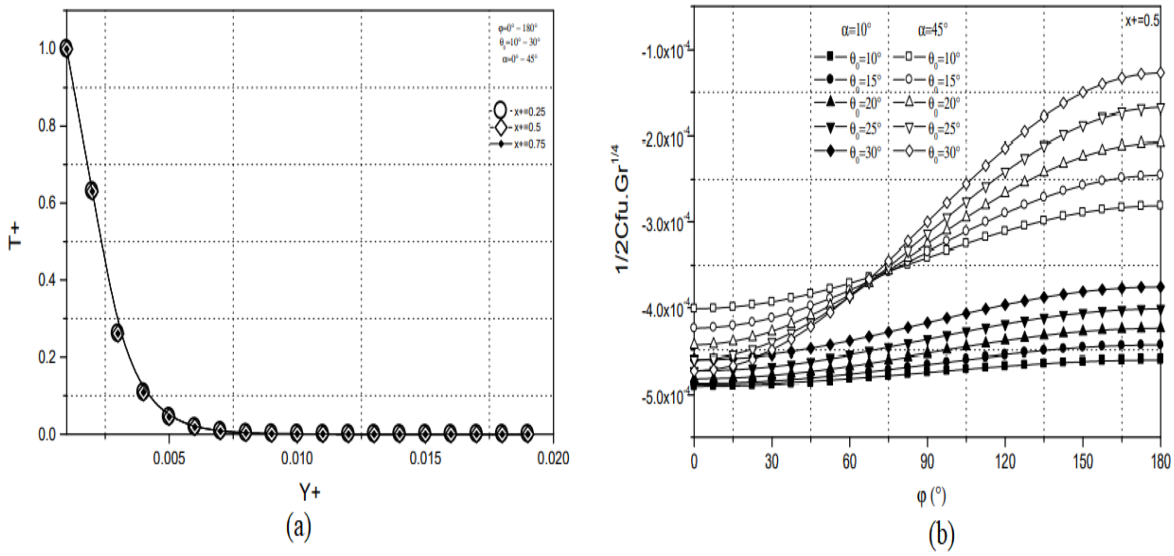

Figure 8. Evolutions of the dimensionless temperature T+ and the meridian or tangential friction coefficient
(a) : T+ against y+, x+=0.25, 0.5, 0.75, α=0°-45°, θ_0=10°-30° and φ=0°-180°
(b) : Cf_u against φ, α=10° and 45°, θ_0=10°- 30°

In this work, we limit ourselves to the opening of the body, contributing to the aerodynamic performance mentioned previously to our research question. The neutral point represented by the independence of the dimensionless quantity indicates the starting point and inversion of intensity, and in this point, the physical parameters have no influence on this quantity. During the exploration of the results, this point is visible at certain moments and almost on all dynamic quantities, and very little on thermal ones. Its azimuthal position is near 90° and this is proportional to the limit value of the aperture (figure 9.a and 9.b). The lower optimal value is around 60°. So, the performance values are in an interval of 60° to 90°. Beyond these, the stability condition begins to be broken, the profile studied can no longer fulfill its role of channeling the flow, of regulating the central air flow towards the sensor.

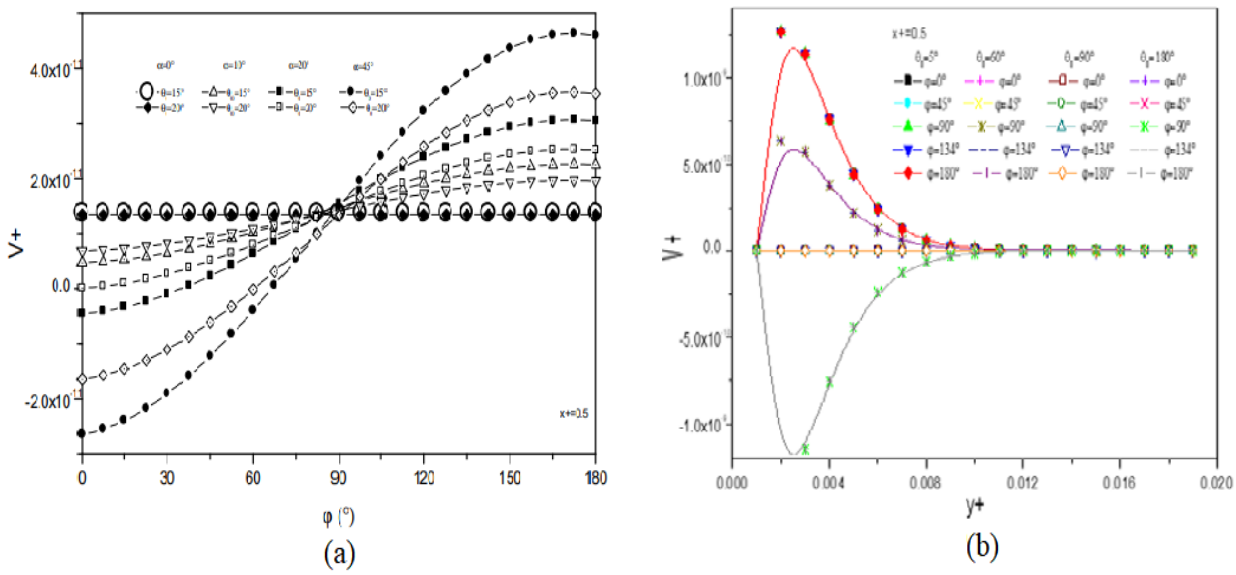

Figure 9. Evolutions of the dimensionless normal component V+ as a function of the dimensionless azimuthal and normal coordinates
(a) : V+ against φ, α=0°, 10°, 20°, 45°, θ_0=15° and 20°
(b) : V+ against y+, φ = 0°, 45°, 90°, 134° and 180°, θ_0= 5°, 60°, 90° and 180°, x+=0.5

VII. CONCLUSION AND PERSPECTIVE

We carried out a numerical study of heat and mass transfer in the boundary layer developed around bodies of revolution immersed in a three-dimensional flow. The conservation equations were solved by an implicit finite-difference scheme associated with the Thomas algorithm. Numerous reviews have been carried out across thousands of results deriving from various cases and several authors to answer a research question offering an alliance between fundamental and applied research. The conical or elliptical shape at the entrance to wind turbines is not a matter of chance, or for aesthetic reasons, but plays a vital role in the stability of the entire aeromechanical wheel.

The recommended optimum range of use, between 60° and 90°, would contribute to the aerodynamic control of the entire aero-motor. In the next paper, however, we offer an ideal best-performing value for this interval.

REFERENCES

[1]. U. Canissius, O. Gastro, D. Tomboravo, E. Razafindrakotomanga and A. S. Tsialefitry, (2023). Wind generator: Importance, limit and performance of the aerodynamic profile at the sensors entrance. American Journal of Engineering Research (AJER), Vol 12, Issue 6, pp. 35-42.

[2]. JUVENT wind turbine erected on site (Mont-Crosin, Switzerland, near Bern): https://www.youtube.com/watch?v=iceJfv58bAQ ; EDF video summarizing how a wind turbine works: https://www.youtube.com/watch?v=v6ZNDQ80ELE. Accessed June 25, 2022.

[3]. Merk, H.J. and Prins, J. A., (1953). Thermal convection in laminar boundary layer. Int. Appl. Sci. Res., 4, pp.11-24.

[4]. M. Alamgir, (1989). Overall heat transfer from vertical cones in laminar free convection: an approximate method. ASME Journal of Heat Transfer, 101, pp. 174-176.

[5]. Bapuji Pullepu, K. Ekambavanan and Ali. J. Chamkha (2007). Unsteady laminar natural convection flow past an isothermal vertical cone. Int. J. Heat and Technology, 25(2), pp.17-28.

[6]. M. A. Hossain and S. C. Paul, (2001). Free convection from a vertical permeable circular cone with nonuniform surface temperature. Acta Mechanica, 151, pp. 103-114.

[7]. Pop and Tsung Yen, (1999). Natural convection over a vertical wavy frustum of a cone. Int. J. Non-linear Mechanics, 34, pp. 925-934.

[8]. Y. C. Ching, (2015). Free convection heat transfert from a non-isothermal. Permeable cone suction and temperature dependent viscosity. Journal of applied Science andEngineering, 18(1), pp. 17-24.

[9]. M. Siabdallah, B. Zeghmati and M. Daguenet. Etude de la convection naturelle thermique et massique dans la couche limite autour d'un tronc de cône à paroi sinusoïdale. 12è Journée Internationale de Thermique, Maroc, 2005.

[10]. H. Abdurrachim. Etude théorique et expérimentale de la convection naturelle laminaire sur des surfaces ondulées. Doctoral thesis, Perpignan University, 1980.

[11]. F. A. Rakotomanga and E. Alidina. Transferts thermiques convectifs tridimensionnels autour d'un cône de révolution. Conference SFT, réf 6212, Gérardmer, France, 2013.

[12]. S. Nadeem, S. Saleem, (2014). Mixed convection flow of Eyring – Powell fluid along a rotating cone", Result in Physics, 4, pp. 54-62.

[13]. Y. Mochimaru. Numerical Simulation of Natural Convection in a Cavity of an Ellipsoid of Revolution, using a Spectral Finite Difference Method. Fourteenth International Conference on Numerical Methods in Fluid Dynamics, India, 453, pp. 485-489, 2005.

[14]. M. Medvinsky, E. Turkel and U. Hetmaniuk, (2008). Local absorbing boundary conditions for elliptical shaped boundaries. JCP, 227(18), pp. 8254-8267.

[15]. N. Souad, C. Mbow, J. H. Lee, W. H. Park and M. Daguenet, (1990). Etude numérique du modèle de Boussinesq de convection naturelle transitoire dans un ellipsoide de révolution de grand axe vertical rempli d'air. JHT, 36(3), pp.224-233.

[16]. N. Souad. Etude numérique de la convection naturelle dans un ellipsoïde de révolution de grand axe vertical et dans un cylindre horizontal de section elliptique. Doctoral thesis, Perpignan University, France, 1996.

[17]. C. Raminosoa, R. Ratobison, A. Ali Cherif, A. Daif and M. Daguenet, (1995) Convection mixte autour d'une sphère, Revue Générale de Thermique.

[18]. E. Alidina. Contribution à l'étude d'une convection mixte tridimensionnelle autour d'une ellipsoïde de révolution dans un écoulement ascendant de fluide newtonien, Doctoral thesis, Antananarivo University, Madagascar, 1997.

[19]. G. Le Palec. (1986) Etude de la convection mixte tridimensionnelle autour d'une sphère en rotation dans un écoulement ascendant de fluide newtonien. Doctoral thesis, Perpignan University, 1986.

[20]. D. Ouldhadda, Etude de la convection mixte autour d'un corps à symétrie de révolution d'axe vertical en rotation en présence d'un écoulement forcé axial et d'une convention naturelle, Doctoral thesis, Perpignan University, France, 1991.

[21]. U. Canissius, F. A. Rakotomanga and E. Alidina (2015). Etude numérique de la convection naturelle tridimensionnelle autour d'un cône de révolution inclinée. Afrique SCIENCE 11(1), pp. 1-11.

[22]. G. Bezandry, (2017.a). Influence de l'ouverture du sommet sur la convection rotatoire pure autour d'un cône de révolution. AfriqueSCIENCE, 13(3), pp.251 - 261.

[23]. G. Bezandry,R. Randrianarivelo, C. Leticia, E. K.Mourtallah-x, U.Canissius and E.Alidina,(2017.b). Influence de l'écoulement forcée sur la convection rotatoire autour d'un cône de révolution. AfriqueSCIENCE, 13(4), pp. 357 - 368.

[24]. E. Mourtallah-x, F. A. Rakotomanga, U. Canissius and E. Alidina, (2019). Numerical study of the three-dimensional mixed convection around an inclined cone of revolution. American Journal of Engineering Research, 8(5), pp. 150-160.

[25]. R. Randrianarivelo, G. Bezandry, U. Canissius and E. Alidina, (2017). Convection mixte tridimensionnelle, naturelle et rotatoire autour d'un cône. Afrique SCIENCE, 13(5), pp. 150-160.

[26]. R. Randrianarivelo, G. Bezandry, U. Canissius and E. Alidina, (2018). Étude d'une convection mixte tridimensionnelle naturelle et rotatoire autour d'un cône incliné. Afrique SCIENCE, 14(1), pp. 281-291.

[27]. C. Leticia, U. Canissius and E. Alidina, (2020). Forced and Rotary Convection around a Cone of Revolution. American Journal of Engineering Research, 9(11), pp. 48-53.

[28]. F. N. Lin, (1976). Laminar convection from a vertical cone with uniform surface heat flux. Letters in Heat and Mass Transfer, 3, pp. 49–58.

[29]. M. K. Jaman and M. A. Hossain, (2010). Effect of Fluctuating Surface Temperature on Natural Convection Flow Over Cylinders of Elliptic Cross Section. OTPJ, 2, pp. 35-47.

[30]. J.H. Merkin, (1977). Free convection boundary layers on cylinders of elliptic cross section, ASME JHT, 99, pp. 453–457.

[31]. U. Canissius, (2016). Convection naturelle tridimensionnelle autour d'un cône de révolution inclinée. Doctoral thesis, Antsiranana University, p. 202, Madagascar.